Int J Adv Manuf Technol (2017) 92:3991–3999
DOI 10.1007/s00170-017-0456-1

ORIGINAL ARTICLE

Multi-objective optimization of variable packing pressure profile and process parameters in plastic injection molding for minimizing warpage and cycle time

Satoshi Kitayama[1] · **Masaki Yokoyama**[2] · **Masahiro Takano**[3] · **Shuji Aiba**[4]

Received: 22 February 2017 / Accepted: 24 April 2017 / Published online: 7 May 2017

Abstract Process parameters in plastic injection molding (PIM) such as the packing pressure, the melt temperature, and the cooling time have a direct influence on the product quality. It is important to determine the optimal process parameters for high product quality. In addition to the product quality, high productivity is required to plastic products. This paper proposes a method to determine the optimal process parameters in the PIM for high product quality and high productivity. A constant packing pressure during the PIM is conventionally used, but the variable packing pressure profile that the packing pressure varies in the packing phase is adopted as the advanced PIM. Warpage and cycle time are taken as the product quality and the productivity, respectively. Then, these are simultaneously minimized and the pareto-frontier between them is identified. Numerical simulation in the PIM is so intensive that a sequential approximate optimization using radial basis function is adopted. It is found through the numerical result that the variable packing pressure profile can improve both the warpage and the cycle time, compared with the conventional PIM approach. In order to examine the validity of the proposed approach, the experiment is carried out. It is confirmed through the numerical and experimental results that the proposed approach is valid for minimizing the warpage and the cycle time.

Keywords Plastic injection molding · Variable packing pressure profile · Multi-objective optimization · Sequential approximate optimization

✉ Satoshi Kitayama
kitayama-s@se.kanazawa-u.ac.jp

Masaki Yokoyama
makkey.yoko@stu.kanazawa-u.ac.jp

Masahiro Takano
takano@irii.jp

Shuji Aiba
aibas@sodick.co.jp

[1] Kanazawa University, Kakuma-machi, Kanazawa 920-1192, Japan

[2] Graduate School of Natural Science & Technology, Kanazawa University, Kakuma-machi, Kanazawa 920-1192, Japan

[3] Industrial Research Institute of Ishikawa, 2-1, Kuratsuki, Kanazawa 920-8203, Japan

[4] Sodick Co., Ltd., Ka-1-1, Miya-machi, Kaga-shi, Ishikawa 922-0595, Japan

1 Introduction

Plastic injection molding (PIM) is one of the important industrial technologies to produce plastic products with high productivity. Plastic products have several advantages, such as light weight, high stiffness, and good appearance. In the PIM, to smoothly flow melt plastic into the cavity, the mold is heated. The melt plastic is then filled into the cavity with injection pressure and is packed with high packing pressure for the desirable shape. Finally, the melt plastic is cooled down for solidification, and the solid plastic product is ejected. The low injection pressure, the short injection time, and the low mold temperature will easily lead to short shot that the melt plastic is not filled into the cavity, and the low packing pressure and the short cooling time will cause warpage that is one of the major defects in the PIM. Cooling time has a significant influence on not only the productivity but also the product quality. Therefore, the process parameters in the PIM such as the melt temperature, the injection pressure, the packing pressure, and the cooling time should be adjusted and optimized for high product quality as well as high productivity. To

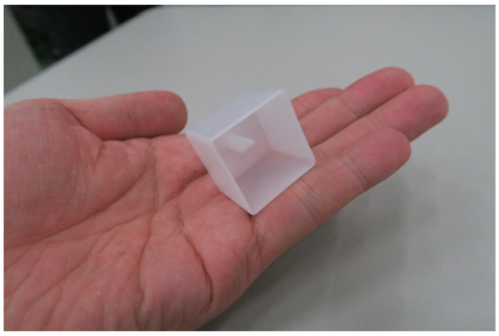

Fig. 1 Box-type plastic product

determine the process parameters for successful PIM, a trial and error method is widely used. Due to the recent advance of computer technology, computer-aided engineering (CAE) coupled with design optimization is recognized as an alternative approach for determining the optimal process parameters. In general, the numerical simulation of PIM is so intensive that a response surface is valid. In particular, a sequential approximate optimization (SAO) that the response surface is repeatedly constructed and optimized is recognized as one of the powerful tools available, and the general framework of the process parameter optimization in PIM is well summarized in Ref. [1]. Here, let us briefly review the representative papers related to the process parameter optimization using response surface.

Early work on the process parameters in the PIM can be found in Ref. [2], in which the neural network was used for the response surface and the genetic algorithm was applied for the determination of the optimal process parameters. Kurtaran et el. determined the optimal process parameters to minimize the warpage of bus ceiling lamp base [3], in which they first conducted the analysis of variance based on the numerical simulations. After that, several significant process parameters

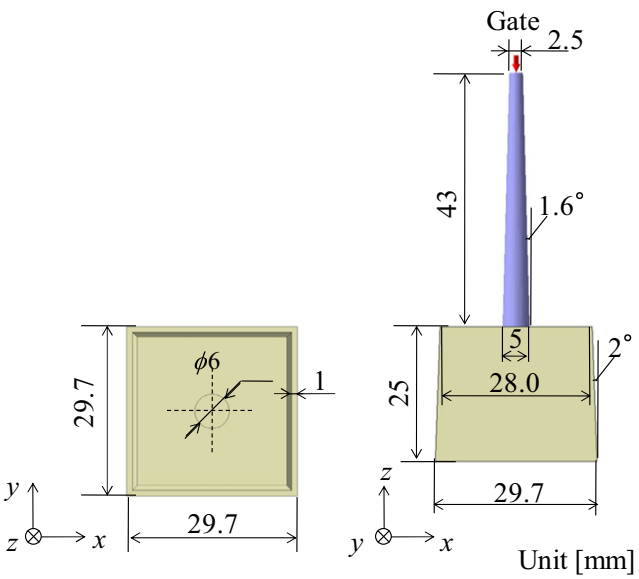

Fig. 2 Detailed dimensions of plastic product

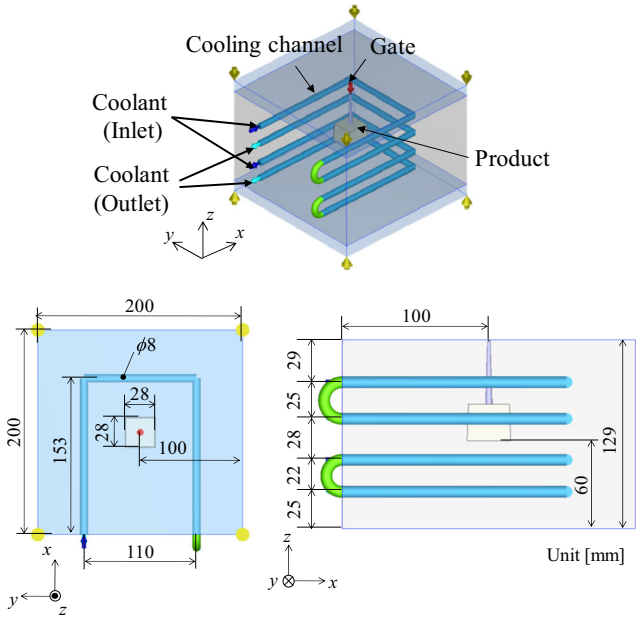

Fig. 3 Overview of mold and cooling channel

were selected and the response surface using the quadratic polynomial was used to determine the optimal process parameters. Similar approach can be found in Ref. [4], in which the neural network was used to approximate the warpage of PC button base and the optimal process parameters were determined. Shen et al. also adopted the neural network and the genetic algorithm to determine the optimal process parameters for minimizing the sink mark of refrigerator top cover [5]. Unlike Refs. [2–4], the approximation by the neural network and the optimization by the genetic algorithm were iterated till a criterion was satisfied. Note that this approach does not belong to the SAO. Gao and Wang adopted the SAO using the Kriging to determine the optimal process parameters for the warpage minimization of cellular phone cover [6]. They also adopted the SAO to determine the optimal packing profile and the optimal process parameters for warpage minimization [7]. Though a constant packing pressure is so widely used in other works [8–12], the variable packing pressure profile that

Table 1 Material property of polyacetal resin

Melt density [g/cm^3]	1.19
Solid density [g/cm^3]	1.4
Eject temperature [°C]	135
Maximum shear stress [MPa]	56
Thermal conductivity [W/(m °C)]	0.336
Elastic module [GPa]	2.8
Poisson ratio	0.38
Specific heat [J/(kg °C)]	2503
Material characteristics	Crystalline
Recommended mold temperature [°C]	60–120
Recommended melt temperature [°C]	180–210

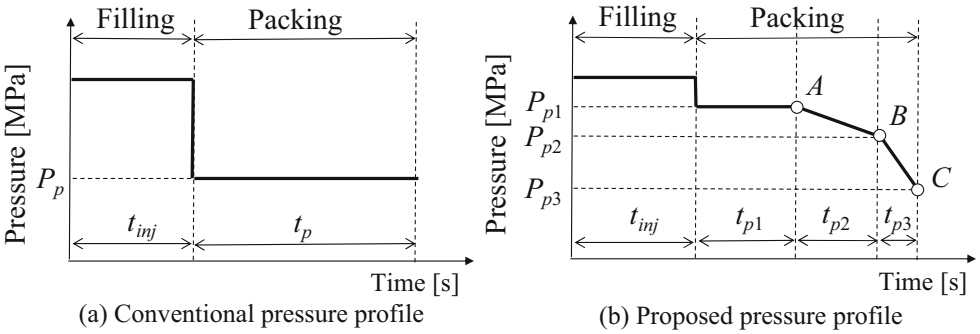

Fig. 4 Difference between conventional and proposed packing pressure profiles

the packing pressure is varied in the packing phase is directly optimized unlike others. After this work, Li et al. performed the optimization of variable packing pressure profile for the shrinkage evenness of a slab [13]. It is clear from Refs. [7, 13] that not only the process parameters but also the packing pressure profile have a significant influence on the product quality. Note that the validity of the variable packing pressure profile was discussed and the cycle time was not taken into account in Refs. [6, 7, 13].

High dimensional accuracy is required to plastic products, and the major concern is to minimize defects such as warpage, sink mark, and volume shrinkage. In addition to these defects, the high productivity is required in PIM. Zhao et al. minimized the cooling time for the high productivity [14], in which two objective functions (the cavity pressure for warpage minimization, and the temperature difference at the end of filling for shrinkage minimization) were minimized. The weighted sum was adopted to minimize all objective functions, and pareto-optimal solutions were determined. Chen et al. minimized (1) the maximum difference of the volume shrinkage, (2) the total volume of runner system, and (3) the cycle time [15], in which the cycle time was calculated by the sum of injection time, packing time, and cooling time. The pareto-frontier among three objective functions was then identified with the genetic algorithm. In general, long cooling time and packing time lead to high product quality but result in long cycle time. On the other hand, short cooling time and packing time easily cause defects such as warpage and volume shrinkage. Therefore, the trade-off between the product quality and the cycle time can be observed. When the injection time, the packing time, and the cooling time are handled as the process parameters, the cycle time should always be taken into account.

Here, the main issues discussing in this paper are summarized as follows:

1. High product quality is always required in the plastic products. In the case of thin plastic product, the warpage that is one of the major defects should be minimized.
2. In addition to the warpage minimization, the cycle time is one of the crucial factors for the high productivity. In other words, the cycle time should also be minimized for the high productivity.
3. The variable packing pressure profile clearly affects the warpage and the cycle time. In addition to the variable packing pressure profile, several process parameters such as the melt temperature and the cooling temperature of coolant should be optimized.
4. It is important to examine the validity of the optimal packing pressure profile through both the numerical simulation and the experiment.

In this paper, a multi-objective optimization of variable packing pressure profile and process parameters for minimizing warpage and cycle time is performed. In general, the numerical simulation in PIM is so intensive that the SAO is adopted for the optimization. One of the authors has already developed the SAO using a radial basis function (RBF) network [16, 17], and this is used as a design optimization tool. Based on the numerical result, the validity of the proposed approach is examined through the experiment (GL30-LP, Sodick).

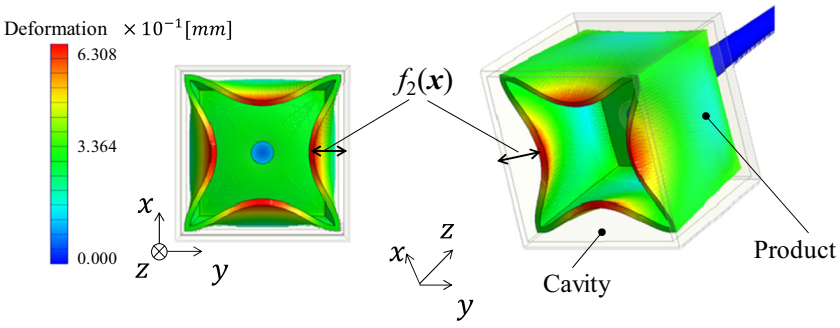

Fig. 5 Illustrative example of warpage of box-type product (×10)

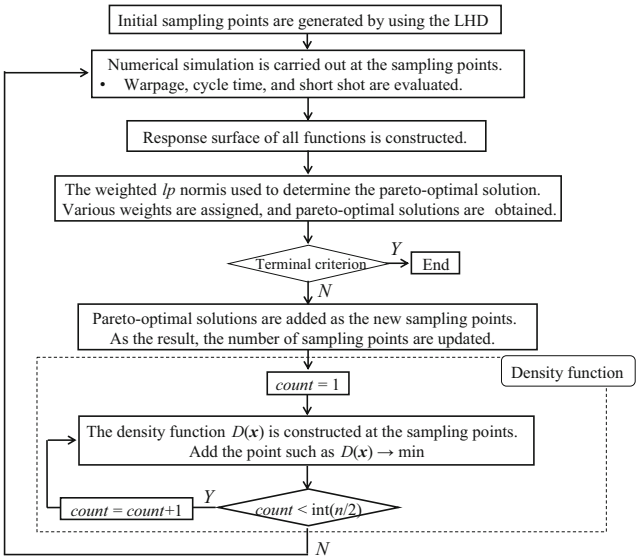

Fig. 6 Sequential approximate optimization algorithm for multi-objective optimization

The rest of this paper is organized as follows: In Section 2, the numerical simulation model considering in this paper is described. In Section 3, the multi-objective design optimization is formulated. The design optimization procedure is also described in this section. Numerical simulation using the SAO using RBF network is carried out and the result is shown in Section 4. Based on the numerical result, the experiment is carried out. Moldex3D (R13) is used for the numerical simulation. See the Appendix about the SAO system using the RBF network.

2 Numerical simulation model

The target plastic product is shown in Fig. 1, and the detailed dimensions are shown in Fig. 2. The thickness is 1 mm, the height of the product is 25 mm, and the width is 29.7 mm. The overview of the molding die and the cooling channel is shown in Fig. 3, where two inlets and outlets are equipped and the diameter of cooling channel is set to 8 mm. In the numerical simulation, the mold temperature is set to 90 °C. The polyacetal resin (POM) is used, and its material property is listed in Table 1.

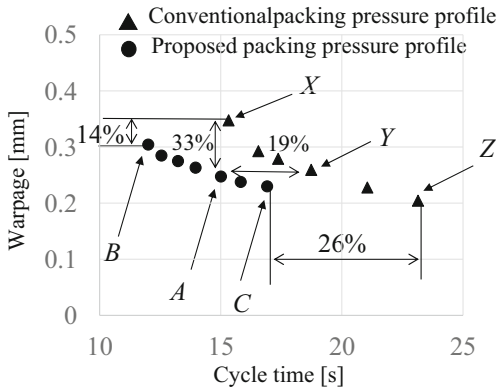

Fig. 7 Difference of pareto-frontier

3 Multi-objective optimization for minimizing warpage and cycle time

3.1 Multi-objective optimization

In general, a multi-objective optimization (MOO) problem is formulated as follows [18]:

$$\left.\begin{array}{l}(f_1(\boldsymbol{x}), f_2(\boldsymbol{x}), \cdots, f_K(\boldsymbol{x})) \rightarrow \min \\ x_i^L \le x_i \le x_i^U \quad i = 1, 2, \cdots, n \\ g_j(\boldsymbol{x}) \le 0 \quad j = 1, 2, \cdots, ncon\end{array}\right\} \tag{1}$$

where $f_i(\boldsymbol{x})$ is the ith objective function to be minimized, K represents the number of objective functions, x_i denotes the ith design variable, x_i^L and x_i^U are the lower and upper bounds of the ith design variable, n represents the number of design variables, $g_j(\boldsymbol{x})$ denotes the jth design constraint, and $ncon$ represents the number of design constraints.

3.2 Design variables

In this paper, the variable packing pressure profile and four process parameters (the melt temperature (T_{melt}), the injection time (t_{inj}), the cooling temperature of coolant (T_c), and the cooling time (t_c)) are taken as the design variables. Let us explain about the variable packing pressure profile using Fig. 4, in which the horizontal axis represents the time, and the vertical one the pressure, respectively. Figure 4a shows the conventional packing pressure profile during the PIM process, from which it is found that a constant packing pressure is used. In the conventional approach, the packing pressure (P_p) and the packing time (t_p) should be optimized. Therefore, in this case, the design variables are $\boldsymbol{x} = (T_{\mathrm{melt}}, t_{\mathrm{inj}}, P_p, t_p, T_c, t_c)^T$.

Next, let us explain about the proposed packing pressure profile shown in Fig. 4b, from which it is clear that the pressure profile varies according to the time unlike the conventional one. Unlike Refs. [6, 7, 13], the proposed packing pressure profile consists of six parameters (the packing pressure P_{pi} and the packing time t_{pi} (i = 1,2,3) at points A, B, and C in Fig. 4b). Therefore, in this case, the design variables are $\boldsymbol{x} = (T_{\mathrm{melt}}, t_{\mathrm{inj}}, P_{p1}, P_{p2}, P_{p3}, t_{p1}, t_{p2}, t_{p3}, T_c, t_c)^T$.

Note that it is possible to handle the injection pressure as the design variables. However, it is difficult to set up the injection pressure exactly in the experiment. Inappropriate injection pressure easily leads to short shot. In order to avoid the short shot, a constant injection pressure (200 MPa) is used in both the numerical simulation and the experiment.

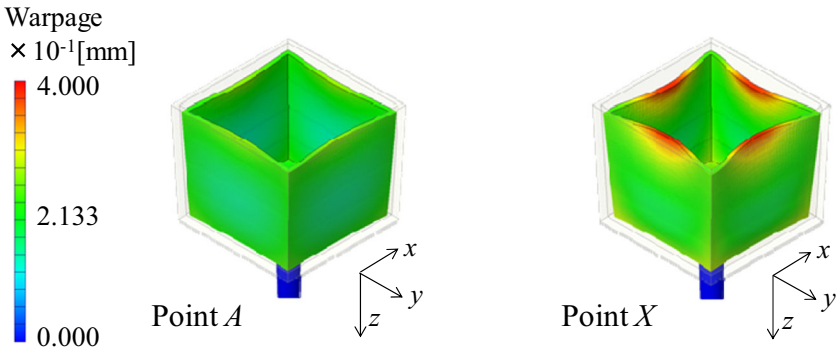

Fig. 8 Deformation at points A and X

3.3 Objective functions

As described in Section 1, the short cycle time is always important in the PIM for the high productivity. In this paper, the cycle time is taken as the first objective function $f_1(\boldsymbol{x})$ and is simply calculated as follows:

a. *In the case of conventional packing pressure profile*

$$f_1(\boldsymbol{x}) = t_{\text{inj}} + t_p + t_c \rightarrow \min \tag{2}$$

b. *In the case of proposed packing pressure profile*

$$f_1(\boldsymbol{x}) = t_{\text{inj}} + t_{p1} + t_{p2} + t_{p3} + t_c \rightarrow \min \tag{3}$$

Next, the warpage is taken as the second objective function $f_2(\boldsymbol{x})$ for the high product quality. In the case of the box-type plastic product, as shown in Fig. 5, the warpage is evaluated as the maximum deformation. Therefore, the maximum distance between the cavity and the product after eject is taken as the second objective function.

3.4 Sequential approximate optimization for multi-objective optimization

In this paper, two objective functions (cycle time and warpage) are minimized. Therefore, the objective is to identify the pareto-frontier between the cycle time and the warpage. The SAO system using the RBF network proposed by one of the authors is used to identify the pareto-frontier with a small number of simulations. In this section, the procedure is briefly described. In the Appendix, the key points in the SAO system using the RBF network are described.

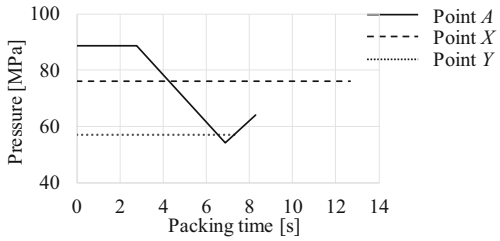

Fig. 9 Difference of packing pressure profile between proposed and conventional approaches

(STEP 1) The Latin hypercube design (LHD) is used to generate some initial sampling points (LHD).

(STEP 2) Through the numerical simulation using Moldex3D (R13), the objective functions (cycle time and warpage) are numerically evaluated at the sampling points.

(STEP 3) All functions are approximated by the RBF network. Here, the approximated objective functions are denoted as $\tilde{f}_i(\boldsymbol{x})$ $(i = 1, 2, \cdots, K)$.

(STEP 4) The pareto-optimal solutions of response surface are determined by using the weighted *lp* norm method formulated as follows:

$$\left[\sum_{i=1}^{K}\left(\alpha_i \tilde{f}_i(\boldsymbol{x})\right)^p\right]^{1/p} \rightarrow \min \tag{4}$$

where $\alpha_i (i = 1, 2, \cdots, K)$ represents the weight of the *i*th objective function, and p is the parameter. In this paper, p is set to 4. In order to obtain a set of pareto-optimal solutions, various weights are assigned.

(STEP 5) If terminal criterion is satisfied, the SAO algorithm will be terminated. Otherwise, the pareto-optimal solutions are added as the new sampling points. As a result, the number of sampling points is updated.

(STEP 6) The density function is constructed and minimized. The optimal solution of the density function is added as a new sampling point. This step is repeated till a terminal criterion is satisfied. See the Appendix for the detail of the density function.

(STEP 7) Return to STEP 2.

Figure 6 shows the flow of the SAO algorithm for MOO. For better understanding, let us describe the density function part in Fig. 6. The density function is repeatedly constructed and minimized, as shown in Fig. 6 where the parameter count

Table 2 Comparison of cycle time between points A, X, and Y

	t_{inj} [s]	t_p [s]			$t_{c\ [s]}$	$f_i(x)$
Point A	0.25	2.78	4.08	1.41	6.83	15.35
Point X	0.37	12.67			1.70	14.74
Point Y	0.64	7.49			10.80	18.93

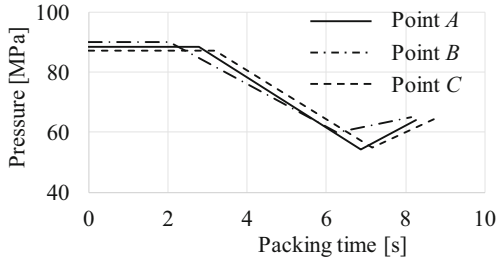

Fig. 10 Comparison among packing pressure profile among points A, B, and C

is introduced in this phase. This parameter controls the number of sampling points with which the density function is constructed. Thus, in the algorithm, the number of sampling points by the density function varies according to the number of design variables. If the parameter *count* is less than int(n/2), this parameter is increased as *count* = *count* + 1. The terminal criterion in this part is given by int(n/2), where int() represents the rounding-off. We expect that iterative use of the density function will yield a uniform distribution of sampling points. As the terminal criterion in STEP 5, the error at the pareto-optimal solutions is handled. The error at the pareto-optimal solutions in STEP 4 is within 5%; the SAO algorithm will be terminated.

4 Numerical and experimental results

First, the numerical simulation is carried out in order to identify the pareto-frontier. After that, the experiment based on the numerical result is carried out. The lower and upper bounds of the design variables in each case are set as follows:

a. *In the case of conventional packing pressure profile*

$$\begin{array}{lll} 180 \le T_{\mathrm{melt}} \le 210\,[^{\circ}\mathrm{C}] & 0.1 \le t_{\mathrm{inj}} \le 1.0\,[\mathrm{s}] & 50 \le P_p \le 100\,[\mathrm{MPa}] \\ 1.0 \le t_p \le 20.0\,[\mathrm{s}] & 40 \le T_c \le 90\,[^{\circ}\mathrm{C}] & 1.0 \le t_c \le 40.0\,[\mathrm{s}] \end{array} \quad (5)$$

b. *In the case of proposed packing pressure profile*

$$\begin{array}{lll} 180 \le T_{\mathrm{melt}} \le 210\,[^{\circ}\mathrm{C}] & 0.1 \le t_{\mathrm{inj}} \le 1.0\,[\mathrm{s}] & 50 \le P_{p1}, P_{p2}, P_{p3} \le 100\,[\mathrm{MPa}] \\ 1.0 \le t_{p1} \le 10.0\,[\mathrm{s}] & 1.0 \le t_{p2}, t_{p3} \le 5.0\,[\mathrm{s}] & 40 \le T_c \le 90\,[^{\circ}\mathrm{C}] \\ 1.0 \le t_c \le 40.0\,[\mathrm{s}] & & \end{array} \quad (6)$$

Fifteen initial sampling points are generated in the case of the conventional packing pressure profile, whereas 20 initial sampling points are generated in the case of the proposed one. Then, the pareto-frontier is identified. In order to identify the pareto-frontier, 42 simulation runs are required in both cases. The pareto-frontier is shown in Fig. 7, in which the black circles denote the pareto-frontier by the proposed packing pressure profile, and the black triangles the one by the conventional packing pressure profile, respectively. It is clear from Fig. 7 that the trade-off can be observed between the warpage and the cycle time. In particular, the trade-off curve of the proposed packing pressure profile is improved, compared with the one of the conventional one. With the proposed packing pressure profile, the improvement of 26% can be achieved in the cycle time and the improvement of 14% can be achieved in the warpage. Let us compare the deformation at points A and X where the cycle time is almost the same. The deformation is shown in Fig. 8, from which it is found that the improvement of 33% is achieved in the warpage. The packing pressure profile is shown in Fig. 9, in which the solid line denotes the packing pressure profile at point A and the dashed line the one at point X. At point A, the high packing pressure is applied and the packing pressure gradually decreases. Finally, the packing pressure slightly increases and the packing phase is terminated. High packing pressure helps keep the temperature of melt plastic high, and the melt plastic is gradually cooled down with decreasing the packing pressure. As a result, the warpage reduction can be achieved. On the other hand, the packing time at point X is long, but the cycle time between points A and X is almost the same. Then, we check the cycle time at these points, which is shown in Table 2. It is found from Table 2 that the cooling time at point X is much short. This indicates that the melt plastic is rapidly cooled

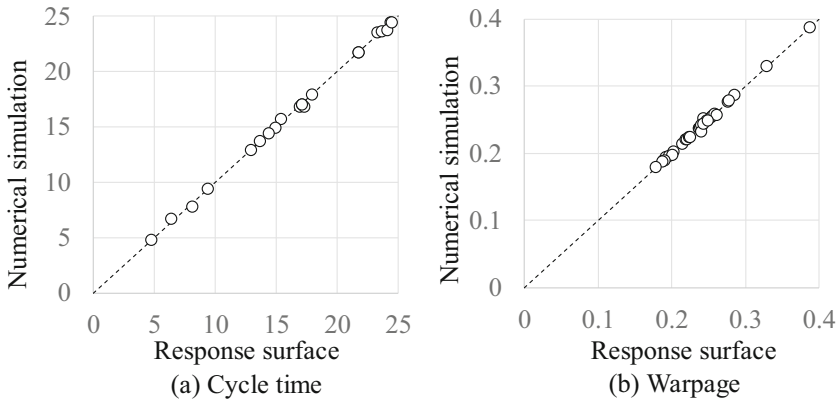

Fig. 11 Accuracy of response surface of the proposed approach

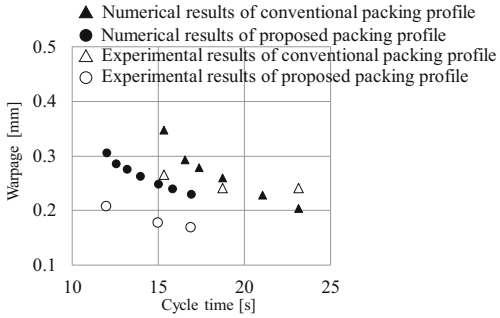

Fig. 12 Experimental results

down and this leads to the large warpage. Next, let us compare the cycle time at points A and Y where the deformation is almost the same. The packing pressure profile at point Y is also shown in Fig. 9 with the dashed line. The packing time at point Y is shorter than the proposed one at point A, but the shorter cycle time is obtained with the proposed packing pressure profile. The pareto-optimal solution at point Y is then compared, which is listed in Table 2. It is found from Table 2 that the injection time and the cooling time at point A are shorter than those at point Y. As a result, the cycle time at point A is improved. Let us compare the packing pressure profiles at points A, B, and C, which are shown in Fig. 10. It is found from Fig. 10 that the packing pressure profiles at these points are similar.

Finally, the accuracy of response surface of the proposed approach is shown in Fig. 11, from which it is found that highly accurate response surface can be obtained. This indicates that highly accurate experimental result will be obtained.

In order to examine the validity of the numerical result, the experiment is carried out at six points shown in Fig. 7 (points A, B, C, X, Y, and Z). The PIM machine (GL30-LP, Sodick) is used in the PIM experiment. The result is shown in Fig. 12, in which the white circles denote the experimental results with the proposed packing pressure profile, and the white triangles the ones with the conventional packing profile. Figure 13 shows one of the proposed packing profiles in the experiment, from which it is clear that the proposed packing pressure is well controlled in the experiment. In addition, it is found from Fig. 12 that the experimental result well agrees with the numerical result. Through numerical and experimental results, the validity of the proposed approach has been confirmed.

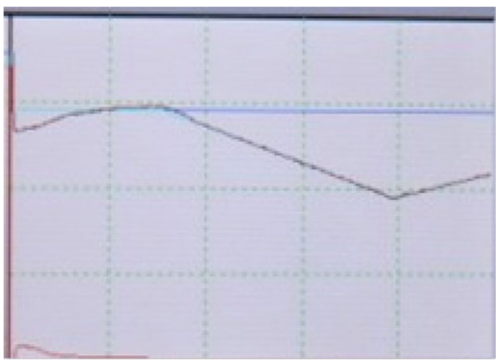

Fig. 13 Variable packing profile in experiment (GL30-LP, Sodick)

5 Conclusions

In this paper, the multi-objective optimization of packing pressure profile and process parameters for minimizing warpage and cycle time is performed. As the advanced PIM, the packing pressure profile that the packing pressure varies in the packing phase is adopted and optimized. In addition to the packing pressure profile, the melt temperature, the injection time, the cooling temperature of coolant, and the cooling time are taken as the process parameters and optimized. The numerical simulation in PIM is so intensive that a sequential approximate optimization using radial basis function is adopted. Through the numerical result, the pareto-frontier between the warpage and the cycle time is identified. In order to examine the validity of the numerical result, the experiment is carried out. The experimental result well agrees with the numerical result. Through numerical and experimental results, the validity of the proposed approach for minimizing the warpage and the cycle time has been confirmed.

Appendix

Radial basis function network

The RBF network is a three-layer feed-forward network. Let $\{\boldsymbol{x}_j, y_j\}$ $(j = 1, 2, \cdots, m)$ be the training data, where m represents the number of sampling points. The response surface is given by

$$\hat{y}(\boldsymbol{x}) = \sum_{j=1}^{m} w_j K(\boldsymbol{x}, \boldsymbol{x}_j) \tag{7}$$

where $K(\boldsymbol{x}, \boldsymbol{x}_j)$ is the jth basis function, and w_j denotes the weight of the jth basis function. Gaussian kernel given by Eq. (8) is generally used in this paper.

$$K(\boldsymbol{x}, \boldsymbol{x}_j) = \exp\left(-\frac{(\boldsymbol{x}-\boldsymbol{x}_j)^T(\boldsymbol{x}-\boldsymbol{x}_j)}{r_j^2}\right) \tag{8}$$

In Eq. (8), $\boldsymbol{x}_j$ represents the jth sampling point, and r_j is the width of the jth basis function. The response y_j is calculated at the sampling point $\boldsymbol{x}_j$. In the RBF network, the following equation is minimized:

$$E = \sum_{j=1}^{m} \left(y_j - \hat{y}(\boldsymbol{x}_j)\right)^2 + \sum_{j=1}^{m} \lambda_j w_j^2 \rightarrow \min \tag{9}$$

where the second term is introduced for the purpose of the regularization. It is recommended that λ_j in Eq. (9) is sufficient small value (e.g., $\lambda_j = 1.0 \times 10^{-2}$). The necessary condition of Eq. (9) results in the following equation.

$$\boldsymbol{w} = \left(\boldsymbol{H}^T\boldsymbol{H} + \boldsymbol{\Lambda}\right)^{-1}\boldsymbol{H}^T\boldsymbol{y} \tag{10}$$

where $\boldsymbol{H}$, $\boldsymbol{\Lambda}$, and $\boldsymbol{y}$ are given as follows:

$$\boldsymbol{H} = \begin{bmatrix} K(\boldsymbol{x}_1,\boldsymbol{x}_1) & K(\boldsymbol{x}_1,\boldsymbol{x}_2) & \cdots & K(\boldsymbol{x}_1,\boldsymbol{x}_m) \\ K(\boldsymbol{x}_2,\boldsymbol{x}_1) & K(\boldsymbol{x}_2,\boldsymbol{x}_2) & \cdots & K(\boldsymbol{x}_2,\boldsymbol{x}_m) \\ \vdots & \vdots & \ddots & \vdots \\ K(\boldsymbol{x}_m,\boldsymbol{x}_1) & K(\boldsymbol{x}_m,\boldsymbol{x}_2) & \cdots & K(\boldsymbol{x}_m,\boldsymbol{x}_m) \end{bmatrix} \tag{11}$$

$$\boldsymbol{\Lambda} = \begin{bmatrix} \lambda_1 & 0 & \cdots & 0 \\ 0 & \lambda_2 & \cdots & 0 \\ \vdots & \vdots & \ddots & \vdots \\ 0 & 0 & 0 & \lambda_m \end{bmatrix} \tag{12}$$

$$\boldsymbol{y} = (y_1, y_2, \cdots, y_m)^T \tag{13}$$

The width in the Gaussian kernel plays an important role for good approximation. We have proposed the following simple estimate about the width [16]:

$$r_j = \frac{d_{j,\max}}{\sqrt{n}\sqrt[n]{m-1}} \quad j = 1, 2, \cdots, m \tag{14}$$

where r_j denotes the width of the jth Gaussian kernel, and $d_{j,\max}$ denotes the maximum distance between the jth sampling point and the other sampling points. Equation (14) is applied to each Gaussian kernel individually and can deal with the non-uniform distribution of sampling points.

Density function using RBF network

In the SAO, it is important to find out the unexplored region for global approximation. In order to find out the unexplored region with the RBF network, we have developed a function called the density function [16]. The procedure to construct the density function is summarized as follows:

(D-STEP 1) The following vector $\boldsymbol{y}^D$ is prepared at the sampling points.

$$\boldsymbol{y}^D = (1, 1, \cdots, 1)^T_{m\times 1} \tag{15}$$

(D-STEP 2) The weight vector $\boldsymbol{w}^D$ of the density function $D(\boldsymbol{x})$ is calculated as follows:

$$\boldsymbol{w}^D = \left(\boldsymbol{H}^T\boldsymbol{H} + \boldsymbol{\Lambda}\right)^{-1}\boldsymbol{H}^T\mathbf{y}^D \tag{16}$$

(D-STEP 3) The density function $D(\boldsymbol{x})$ is minimized.

$$D(\boldsymbol{x}) = \sum_{j=1}^{m} w_j^D K\left(\boldsymbol{x}, \boldsymbol{x}_j\right) \rightarrow \min \tag{17}$$

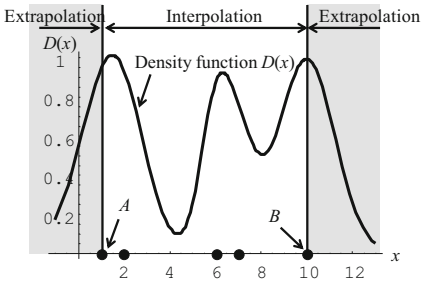

Fig. 14 Illustrative example of density function

(D-STEP 4) The point minimizing $D(\boldsymbol{x})$ is taken as the new sampling point.

Figure 14 shows an illustrative example in one dimension, and the black dots denote the sampling points. It is found from Fig. 14 that local minima are generated around the unexplored region. By adding the optimal solution of the density function, the uniform distribution of sampling points can be achieved. Note that the RBF network is basically the interpolation between sampling points and points A and B in Fig. 14 are the lower and upper bounds of the design variables of the density function.

References

1. Dang XP (2014) General frameworks for optimization of plastic injection molding process parameters. Simulation and Modelling Practice and Theory 41:15–27
2. Shi F, Lou ZL, Lu JG, Zhang YQ (2003) Optimisation of plastic injection moulding process with soft computing. Int J Adv Manuf Technol 21:656–661
3. Kurtaran H, Erzurumlu T (2006) Efficient warpage optimization of thin shell plastic parts using response surface methodology and genetic algorithm. Int J Adv Manuf Technol 27:468–472
4. Ozcelik B, Erzurumlu T (2006) Comparison of the warpage optimization in the plastic injection molding using ANOVA, neural network model and genetic algorithm. J Mater Process Technol 171:437–445
5. Shen C, Wang L, Cao W, Wu J (2007) Optimization for injection molding process conditions of the refrigeratory top cover using combination method of artificial neural network and genetic algorithm. Polym-Plast Technol Eng 46:105–112
6. Gao Y, Wang X (2008) An effective warpage optimization method in injection molding based on the Kriging model. Int J Adv Manuf Technol 37:953–960
7. Gao Y, Wang X (2009) Surrogate-based process optimization for reducing warpage in injection molding. J Mater Process Technol 209:1302–1309
8. Chen CP, Chuang MT, Hsiao YH, Yang YK, Tsai CH (2009) Simulation and experimental study in determining injection molding process parameters for thin-shell plastic parts via design of experiments analysis. Expert Syst Appl 36:10752–10759
9. Deng YM, Zhang Y, Lam YC (2010) A hybrid of mode-pursuing sampling method and genetic algorithm for minimization of injection molding warpage. Mater Des 31:2118–2123

10. Shi H, Gao Y, Wang X (2010) Optimization of injection molding process parameters using integrated artificial neural network model and expected improvement function method. Int J Adv Manuf Technol 48:955–962
11. Yin F, Mao H, Hua L (2011) A hybrid of back propagation neural network and genetic algorithm for optimization of injection molding process parameters. Mater Des 32:3457–3464
12. Xia W, Luo B, Liao XP (2011) An enhanced optimization approach based on Gaussian process surrogate model for process control in injection molding. Int J Adv Manuf Technol 56:929–942
13. Li C, Wang FL, Chang YQ, Liu Y (2010) A modified global optimization method based on surrogate model and its application in packing profile optimization of injection molding process. Int J Adv Manuf Technol 48:505–511
14. Zhao P, Zhou H, Li Y, Li D (2010) Process parameters optimization of injection molding using a fast strip analysis as a surrogate model. Int J Adv Manuf Technol 49:949–959
15. Cheng J, Liu Z, Tan J (2013) Multiobjective optimization of injection molding parameters based on soft computing and variable complexity method. Int J Adv Manuf Technol 66:907–916
16. Kitayama S, Arakawa M, Yamazaki K (2011) Sequential approximate optimization using radial basis function network for engineering optimization. Optim Eng 12(4):535–557
17. Kitayama S, Srirat J, Arakawa M, Yamazaki K (2011) Sequential approximate multi-objective optimization using radial basis function network. Struct Multidiscip Optim 48:501–515
18. Miettinen KM (1998) Nonlinear multiobjective optimization. Kluwer Academic Publishers, Dordrecht